Title

Determinants of [Cl-] in recycling and late endosomes and Golgi complex measured using fluorescent ligands.

Journal

The Journal of cell biology, 160(7)

ISSN

0021-9525

Authors

Sonawane, ND
Verkman, AS

Publication Date

2003-03-01

DOI

10.1083/jcb.200211098

Peer reviewed

JCB Article

Determinants of [Cl^-] in recycling and late endosomes and Golgi complex measured using fluorescent ligands

N.D. Sonawane[1,2,3] and A.S. Verkman[1,2,3]

[1]Department of Medicine and [2]Department of Physiology, and [3]Cardiovascular Research Institute, University of California, San Francisco, San Francisco, CA 94143

Chloride concentration ([Cl^-]) was measured in defined organellar compartments using fluorescently labeled transferrin, α_2-macroglobulin, and cholera toxin B-subunit conjugated with Cl^--sensitive and -insensitive dyes. In pulse-chase experiments, [Cl^-] in Tf-labeled early/recycling endosomes in J774 cells was 20 mM just after internalization, increasing to 41 mM over ~10 min in parallel to a drop in pH from 6.91 to 6.05. The low [Cl^-] just after internalization (compared with 137 mM solution [Cl^-]) was prevented by reducing the interior-negative Donnan potential. [Cl^-] in α_2-macroglobulin–labeled endosomes, which enter a late compartment, increased from 28 to 58 mM at 1–45 min after internalization, whereas pH decreased from 6.85 to 5.20. Cl^- accumulation was prevented by bafilomycin but restored by valinomycin. A Cl^- channel inhibitor slowed endosomal acidification and Cl^- accumulation by ~2.5-fold. [Cl^-] was 49 mM and pH was 6.42 in cholera toxin B subunit–labeled Golgi complex in Vero cells; Golgi compartment Cl^- accumulation and acidification were reversed by bafilomycin. Our experiments provide evidence that Cl^- is the principal counter ion accompanying endosomal and Golgi compartment acidification, and that an interior-negative Donnan potential is responsible for low endosomal [Cl^-] early after internalization. We propose that reduced [Cl^-] and volume in early endosomes permits endosomal acidification and [Cl^-] accumulation without lysis.

Introduction

Acidification of the endosomal pathway is important for the internalization and sorting of receptors and ligands, and vesicular fusion (for review see Mellman, 1996; Mukherjee et al., 1997). The determinants of endosomal acidification include the activity of the vacuolar H^+ pump, the ion and H^+ conductances of the endosomal membrane, endosomal buffer capacity, and the activities of other pumps such as the Na^+,K^+ ATPase (Cain et al., 1989; Fuchs et al., 1989a,b; Rybak et al., 1997; Grabe and Oster, 2001). Acidification measurements in isolated endosomes and ion substitution studies in intact cells have suggested an important role for endosomal Cl^- conductance in facilitating endosomal acidification, probably by providing an electrical shunt to permit active H^+ entry (Glickman et al., 1983; Bae and Verkman, 1990; Mulberg et al., 1991; Zen et al., 1992). H^+ leak and K^+ conductance may also be a determinant of acidification in some endosomes and in acidic secretory compartments such as the Golgi complex (Kim et al., 1996; Farinas and Verkman, 1999; Wu et al., 2001). Recently, endosomal Cl^- channels have been identified as members of the ClC protein family (Jentsch et al., 2002). It has been proposed that mutations in ClC proteins cause human disease (e.g., ClC-3, hippocampal degeneration; ClC-5, Dent's disease; and ClC-7, osteopetrosis and retinal degeneration; George, 1998; Piwon et al., 2000; Kornak et al., 2001; Stobrawa et al., 2001) by defective endosomal Cl^- permeability and impaired acidification.

We recently developed a ratioable Cl^--sensitive fluorescent indicator for direct measurement of Cl^- concentration ([Cl^-])* in endosomes labeled by fluid-phase endocytosis (Sonawane et al., 2002). A green-fluorescing Cl^--sensitive chromophore 10,10′-bis[3-carboxypropyl]-9,9′-biacridinium dinitrate (BAC) was conjugated to amino dextran (40 kD) to-

Address correspondence to Alan S. Verkman, Cardiovascular Research Institute, 1246 Health Sciences East Tower, Box 0521, University of California, San Francisco, San Francisco, CA 94143-0521. Tel.: (415) 476-8530. Fax: (415) 665-3847. E-mail: verkman@itsa.ucsf.edu

Key words: endocytosis; transferrin; ratio imaging; chloride channel; cholera toxin

*Abbreviations used in this paper: α_2M, α_2-macroglobulin; BAC, 10,10′-bis[3-carboxypropyl]-9,9′-biacridinium dinitrate; BAC-dextran, BAC-labeled dextran; BAC-dextran-α_2M-TMR, TMR-α2M conjugated to BAC-dextran; BAC-dextran-CTb-TMR, TMR-CTb conjugated to BAC-dextran; BAC-dextran-Tf-TMR, TMR-Tf conjugated to BAC-dextran; [Cl^-], Cl^- concentration; CTb, cholera toxin B subunit; FITC-α2M-TMR, α2M-labeled with FITC and TMR; FITC-Tf-TMR, Tf-labeled with FITC and TMR; MBS, 3-(maleimido)benzoic acid succinimidyl ester; NPPB, 5-nitro-2-(3-phenylpropylamino)benzoic acid; SPDP, *N*-succinimidyl-3-(2-pyridyldithio)propionate; Tf, transferrin; TMR, 5- (and 6) carboxytetramethylrhodamine; TMR-α_2M, TMR-labeled α_2M; TMR-Tf, TMR-labeled transferrin.

gether with the red-fluorescing Cl^--insensitive chromophore 5- (and 6) carboxytetramethylrhodamine (TMR). The principle finding was that endosomal [Cl^-] in two different cell lines increased from ~25 to 60 mM in parallel to a decrease in endosomal pH from 6.95 to 5.30. The low endosomal [Cl^-] of ~20 mM measured at the earliest time point of 1 min was an intriguing observation because the extracellular solution contained 137 mM Cl^-. Although quantitative measurements of endosomal [Cl^-] could be made, the relatively dim BAC fluorescence (even with maximal BAC-dextran labeling and concentration in the internalization solution, 18 mg/ml) and the fluid-phase dye uptake mechanism precluded specific targeting to defined endosomal or secretory compartments, or analysis of the early kinetics of endosomal [Cl^-].

The goal of this paper is to develop ratioable Cl^--sensitive fluorescent ligands for receptor-mediated internalization in order to do the following: (a) measure [Cl^-] in early/recycling and late endosomes; (b) define quantitatively the role of Cl^- conductance in vacuolar acidification; (c) investigate the mechanisms responsible for the low [Cl^-] early after endosome formation; and (d) measure [Cl^-] in Golgi compartments. Transferrin (Tf) and α_2-macroglobulin (α_2M) were chosen as endosomal markers on the basis of a substantial body of evidence that these ligands are targeted by receptor-mediated endocytosis to early/recycling and late endosomes, respectively (Yamashiro et al., 1984; Dautry-Varsat, 1986; Yamashiro et al., 1989; Mukherjee et al., 1997). The cholera toxin B-subunit (CTb) was chosen as a Golgi compartment marker on the basis of data showing efficient Golgi compartment labeling in Vero cells after retrograde transport (Schapiro et al., 1998). The requirements of the indicators included the following: uptake by a receptor-mediated mechanism; bright, long wavelength fluorescence; Cl^- sensitivity in the range 0–100 mM; pH insensitivity; and stability in cells. As in our previous work (Sonawane et al., 2002), BAC was used as the Cl^--sensitive chromophore; however, BAC could not be conjugated to the protein ligands directly because BAC fluorescence was quenched by >90% after conjugation to proteins, even when long spacers were introduced. Our strategy was to synthesize 1:1 covalent conjugates of TMR-labeled ligands with BAC-labeled dextran (BAC-dextran; see Fig. 1 A). Cell labeling with the fluorescent ligands at nanomolar concentrations in the labeling solution gave remarkably brighter endosomes than labeling with high concentrations of the fluorescent dextran, and permitted a pulse-internalization protocol in which perfusate temperature was increased rapidly after cell surface labeling at low temperature. Ratioable, pH-sensitive Tf, α_2M, and CTb ligands were also synthesized to compare endosomal/Golgi compartment [Cl^-] and pH. Our data establish new classes of targetable Cl^- indicators, define the principle determinants of [Cl^-] in early/recycling and late endosomes, and provide the first data on [Cl^-] in the Golgi compartment.

Results

Characterization of fluorescent ligands for receptor-mediated labeling of endosomes and Golgi compartment

The ligands Tf and α_2M were labeled with TMR and conjugated 1:1 with BAC-dextran using an *N*-succinimidyl-3-(2-pyridyldithio)propionate (SPDP) disulfide linker (Fig. 1 A, left). The SPDP disulfide linker has been used for conjugating proteins to carbohydrates and other polymers in endosomal studies (Wagner et al., 1990; Hogemann et al., 2000). The ligand CTb was labeled with TMR and conjugated 1:1 with BAC-dextran by the very stable 3-(maleimido)benzoic acid succinimidyl ester (MBS) thioether linker (Fig. 1 A, right). The fluorescence of the TMR chromophore is red and Cl^--insensitive, whereas the fluorescence of the BAC chromophore is green and Cl^--sensitive. Fig. 1 B shows fluorescence profiles after gel filtration chromatography of TMR-Tf conjugated to BAC-dextran (BAC-dextran-Tf-TMR; left) and TMR-α2M conjugated to BAC-dextran (BAC-dextran-α_2M-TMR; right) as originally purified (top) and after cellular internalization (bottom). Single peaks were

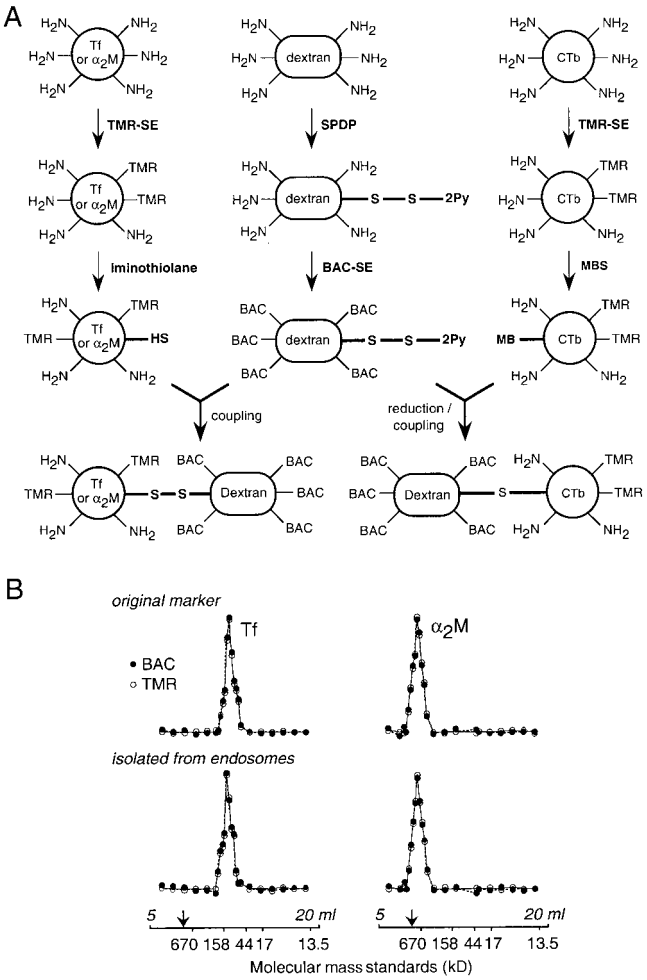

Figure 1. **Synthesis and characterization of fluorescently labeled Cl^--sensing ligands.** (A, left) TMR-labeled Tf and α_2M were conjugated to BAC-dextran by a disulfide linker to generate dual wavelength Cl^- indicators (see Materials and methods). (right) TMR-labeled CTb was conjugated to BAC-dextran by a thioether linker. (B) Elution profiles of BAC-dextran-Tf-TMR (left) and BAC-dextran-α_2M-TMR (right) for gel filtration chromatography on Sephacryl 300HR. Profiles of BAC and TMR fluorescence shown for original purified conjugates (top) and after isolation from cells (bottom) in which endosomes were labeled, chased at 37°C for 15 min (Tf) or 45 min (α_2M), and lysed by sonication and freeze/thaw. Arrow indicates void volume.

seen at apparent molecular sizes of 130 kD (BAC-dextran-Tf-TMR) and 750 kD (BAC-dextran-α_2M-TMR), corresponding to the predicted molecular sizes of the conjugates of 128 and 740 kD, respectively. The BAC and TMR fluorescence of the conjugates comigrated and no fluorescence was seen at lower molecular sizes. These data indicate that the fluorescently labeled ligands consist of 1:1 (mol/mol) ligand–dextran complexes, as engineered, and that they remain stable after endocytosis. Similar experiments indicated stability of the pH indicators (TMR-Tf and TMR-α_2M) and the fluorescent CTb ligands (not depicted).

Fluorescence spectra of BAC-dextran-Tf-TMR, BAC-dextran-α_2M-TMR, and TMR-CTb conjugated to BAC-dextran (BAC-dextran-CTb-TMR) indicated excitation maxima at 365 and 434 nm and emission maximum at 505 nm for BAC, and excitation maximum at 556 nm and emission maximum at 577 nm for TMR (not depicted). BAC fluorescence in the fluorescent ligands was quenched by Cl^- by a collisional mechanism with a Stern-Volmer constant of 36 M^{-1}, whereas TMR fluorescence was not sensitive to Cl^-. Neither BAC nor TMR fluorescence was sensitive to pH (range 4–8), cations, or nonhalide anions including phosphate, bicarbonate, and lactate.

Receptor-mediated endocytosis of Tf and α_2-M conjugates

Fig. 2 shows a series of confocal micrographs of J774 cells after labeling with BAC-dextran-Tf-TMR (A) and BAC-dextran-α_2M-TMR (B). The cell surface was stained after incubation with nanomolar concentrations of fluorescent ligands for 15 min at 4°C (Fig. 2, A and B, 0 min). The green BAC fluorescence was relatively dim because of the high extracellular [Cl^-]. Removal of the internalization solution, cell washing, and warming to 37°C resulted in prompt internalization. The staining pattern of BAC-dextran-Tf-TMR was characteristic of early/recycling endosomes, as also seen for Tf-labeled with FITC and TMR (FITC-Tf-TMR; not depicted). At longer times, there was decreased staining because of ligand recycling to the cell surface. Inclusion of excess unlabeled Tf in the internalization solution blocked BAC-dextran-Tf-TMR binding and uptake (Fig. 2 A, left). In dual-labeling studies, BAC-dextran-Tf-TMR and FITC-TMR-Tf colocalized throughout the chase period (not depicted). For BAC-dextran-α_2M-TMR, there was again a surface pattern initially (Fig. 2 B). Endosomes became brighter and larger over time (as also seen for FITC-TMR-α_2M; not depicted), which is characteristic of ligand transport from early to late endosomes. Excess unlabeled α_2M blocked labeling. In dual-labeling studies, BAC-dextran-α_2M-TMR and FITC-TMR-α_2M colocalized throughout the chase period (not depicted).

[Cl^-] and pH in early/recycling and late endosomes

Calibration of R/G (TMR/BAC fluorescence ratio) versus [Cl^-] was done by incubating dye-loaded cells with high K^+ buffer containing a mixture of ionophores and bafilomycin. Fig. 3 A (left) shows that the dependence of BAC-dextran-Tf-TMR red to green fluorescence ratio (R/G) on [Cl^-] was similar in aqueous solution (closed circles) and in cells (open circles). The kinetics of endosomal [Cl^-] was measured after labeling the cell surface at 4°C followed by rapid warming to 37°C (defined as time 0). Fig. 3 A (right) shows that endosomal [Cl^-] in J774 cells increased from 18 to 40 mM during the 15-min chase period. A similar time course of increasing endosomal [Cl^-] from 24 to 46 mM was found for CHO cells (not depicted). Inclusion of bafilomycin in the extracellular solution reduced endosomal Cl^- accumulation by >50%.

Fig. 3 B (left) shows a pH calibration of FITC-Tf-TMR in cells done using high K^+ buffer containing ionophores

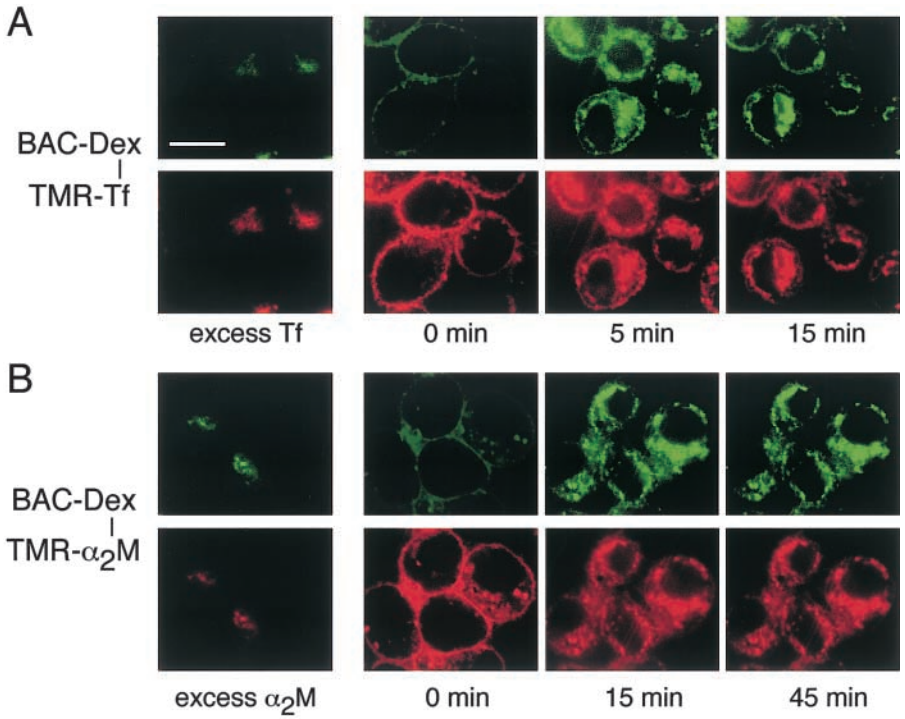

Figure 2. **Confocal microscopy of J774 cells after staining with fluorescently labeled Cl^-sensing ligands.** Micrographs show BAC (green) and TMR (red) fluorescence ligands of Tf (A) and a2M (B). Cells were labeled with 300 nM BAC-dextran-Tf-TMR or 100 nM BAC-dextran-α_2M-TMR for 15 min at 4°C. Micrographs taken before (0 min) and at indicated times after perfusion with 37°C buffer. "Excess Tf" and "excess α_2M" indicate inclusion of 10 μM of the respective unlabeled ligand at the time of incubation with the fluorescent ligand. Bar, 10 μm.

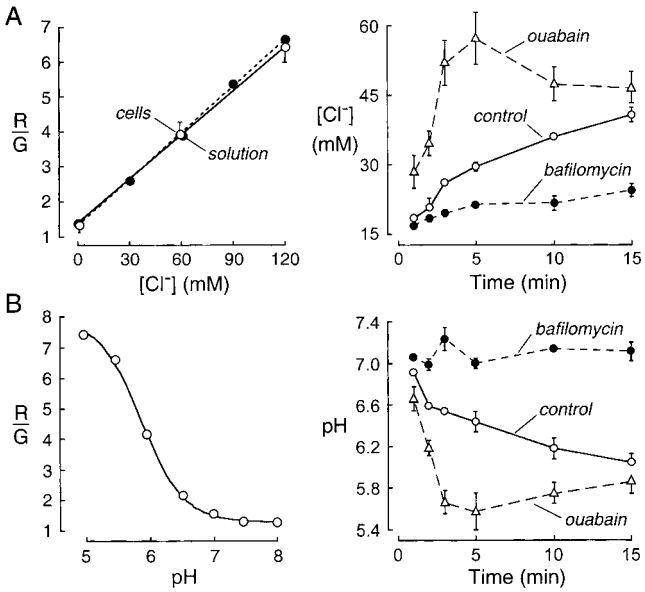

Figure 3. **Kinetics of endosomal [Cl⁻] and pH in Tf-labeled early/recycling endosomes.** (A, left) In situ calibration of BAC-dextran-Tf-TMR red to green fluorescence ratio (R/G) as a function of [Cl⁻] in solution (closed circles) and living cells (open circles). For solution measurements, Cl^- was replaced by NO_3^-. For cell measurements, J774 cells were labeled with BAC-dextran-Tf-TMR for 15 min at 4°C, and incubated for 25 min at 37°C with buffers containing specified [Cl⁻] and ionophores. Data are mean ± SEM for measurements on $n = 4$ separate sets of experiments (10–12 cells from each culture at each time point). (right) Time course of endosomal [Cl⁻] after labeling at 4°C with BAC-dextran-Tf-TMR and perfusion at 37°C ($n = 4$). Where indicated, 200 nM bafilomycin or 200 μM ouabain was present in the incubation solution and perfusate. (B, left) Calibration of FITC-Tf-TMR red to green fluorescence ratio (R/G) as a function of pH ($n = 4$). (right) Time course of endosomal acidification after labeling with FITC-Tf-TMR ($n = 4$).

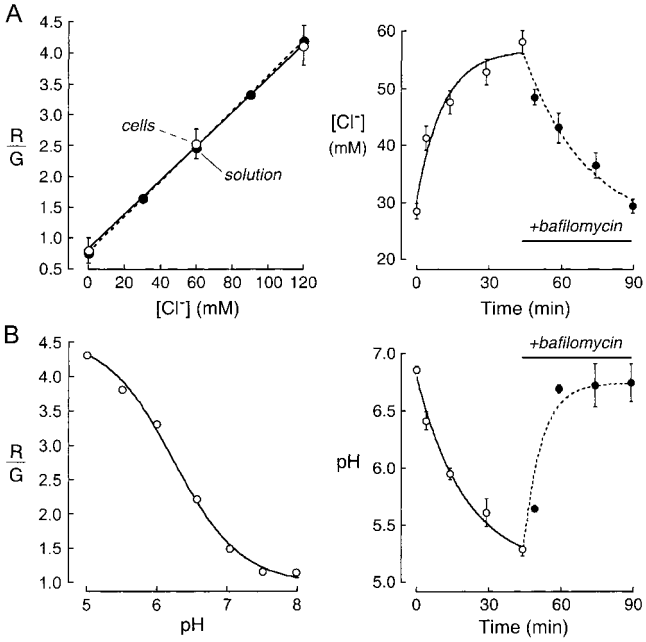

Figure 4. **Kinetics of endosomal [Cl⁻] and pH in α_2M-labeled endosomes.** (A, left) In situ calibration of BAC-α_2M-Tf-TMR red to green fluorescence ratio (R/G) as a function of [Cl⁻] in solution (closed circles) and living cells (open circles; $n = 4$ sets of experiments). (right) Time course of endosomal [Cl⁻] after labeling at 4°C with BAC-dextran-α_2M-TMR and perfusion at 37°C. After the initial chase period of 45 min, 200 nM bafilomycin was added to the perfusate ($n = 4$). (B, left) Calibration of FITC-α_2M-TMR red to green fluorescence ratio (R/G) as a function of pH. (right) Time course of endosomal pH after labeling with FITC-α_2M-TMR. Where indicated 200 nM bafilomycin was added to the perfusate ($n = 4$).

and bafilomycin. R/G (TMR/FITC fluorescence ratio) versus pH was similar in cells and solution. Fig. 3 B (right) shows the kinetics of endosomal acidification measured in parallel experiments using the same experimental protocols as used to measure endosomal [Cl⁻]. Endosomal pH decreased from 6.91 to 6.05 (J774 cells) and 6.95 to 6.18 (CHO cells; not depicted), and was prevented by bafilomycin. We note that in addition to inhibition of the vacuolar H^+ pump, bafilomycin has been shown to inhibit endosomal fusion/trafficking (Van Weert et al., 1995). Inclusion of ouabain in the perfusate produced significantly increased endosomal acidification and parallel Cl^- accumulation (Fig. 3, A and B, right).

Similar kinetic experiments were done for receptor-mediated endocytosis of the fluorescent α_2M-conjugated Cl^- and pH indicators. Fig. 4 A (left) shows that R/G versus [Cl⁻] for BAC-dextran-α_2M-TMR in cells was similar to that in solution. Absolute R/G ratios differed from those in the BAC-dextran-Tf-TMR calibration because of differences in chromophore labeling ratios. Fig. 4 A (right) shows the kinetics of endosomal [Cl⁻] in J774 cells measured from BAC-dextran-α_2M-TMR fluorescence ratios. The increase in [Cl⁻] in BAC-dextran-α_2M-TMR–labeled endosomes was greater than that seen for BAC-dextran-Tf-TMR–labeled endosomes in Fig. 3 A (right). The endosomal [Cl⁻] accumulation was reversed by addition of bafilomycin at 45 min after endocytosis. Interestingly, endosomal [Cl⁻] after bafilomycin became lower (~30 mM) than that in the cytoplasm in these cells (~45 mM). This observation is consistent with coupled H^+/Cl^- exit, though it is difficult to make quantitative predictions because of unknown electrochemical driving forces (membrane potential, $[K^+]$, and $[Na^+]$). For pH measurements, calibrations of endosomal and solution R/G (TMR/FITC fluorescence ratio) for α2M labeled with FITC and TMR (FITC-α_2M-TMR; Fig. 4 B, left) were similar to those in Fig. 3 B (left) for FITC-Tf-TMR. Fig. 4 B (right) shows substantially greater endosomal acidification for FITC-α_2M-TMR–labeled endosomes, which can enter a late endosomal compartment, than for FITC-Tf-TMR–labeled endosomes (Fig. 3 B, right) that remain in an early/recycling compartment. Endosomal acidification was reversed by bafilomycin.

[Cl⁻] and pH in Golgi complex

Fig. 5 A shows labeling of Vero cells by BAC-dextran-CTb-TMR. At time 0 (before warming), a membrane labeling pattern was seen in which the green BAC fluorescence was relatively dim because of the high extracellular [Cl⁻]. Incubation at 37°C resulted in prompt internalization, giving a Golgi compartment staining pattern by 30 min (Fig. 5 A, 45 min). The staining pattern was similar to that reported for internalization of FITC-CTb (Schapiro et al., 1998) and TMR-Verotoxin-B (Schapiro and Grinstein, 2000). The

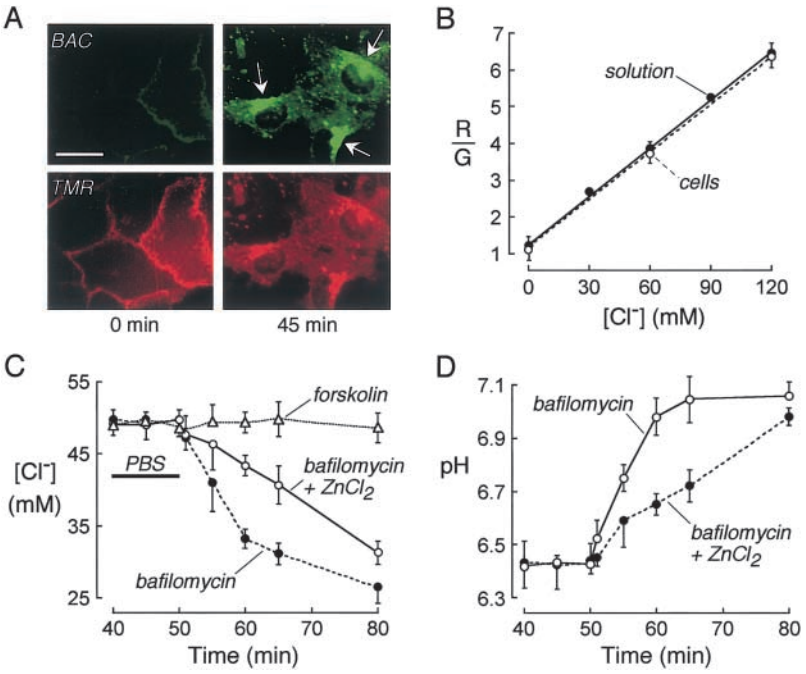

Figure 5. **[Cl⁻] and pH in Golgi compartment of Vero cells.** (A) Cells were labeled with 200 nM BAC-dextran-CTb-TMR for 30 min at 4°C. Micrographs showing BAC (green) and TMR (red) fluorescence taken before (0 min) and at 45 min after perfusion at 37°C. (White arrows) Fluorescently stained Golgi complex. Bar, 10 μm. (B) In situ calibration of BAC-dextran-CTb-TMR red to green fluorescence ratio (R/G) as a function of [Cl⁻] in solution (closed circles) and cells (open circles; $n = 4$). (C) Golgi compartments [Cl⁻]. Where indicated, 200 μM $ZnCl_2$ and/or 200 nM bafilomycin or 10 μM forskolin were present. (D) Time course of Golgi compartment pH in the presence of 200 μM $ZnCl_2$ and/or 200 nM bafilomycin ($n = 4$). Time 0 corresponds to the time of surface labeling.

Golgi compartment staining pattern did not change for >4 h. In dual-labeling studies, BAC-dextran-CTb-TMR and CF-CTb-TMR colocalized in Golgi compartment (not depicted). [Cl⁻] and pH were calibrated in situ as done for the endosome studies (Fig. 5 B, Cl⁻ calibration). Golgi compartment [Cl⁻] was 49 mM and stable for >120 min. Bafilomycin reduced Golgi compartment [Cl⁻] to 26 mM over 30 min (Fig. 5 C), during which time Golgi compartment pH increased from 6.42 to 7.04 (Fig. 5 D). Golgi compartment buffer capacity, as determined from the magnitude of pH increase in response to an NH_4Cl pulse, was 43 mM/pH unit in the pH range of 6.4–7.1. Thus, bafilomycin caused the parallel exit of 26 mM H^+ and 23 mM Cl^-. Inhibition of proton leak by $ZnCl_2$ decreased the rate of Cl^- exit and alkalinization of Golgi compartments after bafilomycin (Fig. 5, C and D). These experiments support the conclusion that the Golgi compartment membrane is H^+ permeable, and that H^+ and Cl^- transport are quantitatively coupled.

Role Cl⁻ conductance in endosomal acidification

Several complementary approaches were used to examine the role of Cl^- conductance in endosomal acidification. First, endosomal Cl^- conductance was partially inhibited by 5-nitro-2-(3-phenylpropylamino)benzoic acid (NPPB) at a high concentration of 100 μM used previously to study the role of Cl^- conductance in acidification of isolated endosomes (Schmid et al., 1989; Busch et al., 1996; Marshansky and Vinay, 1996). Endosomal Cl^- accumulation (Fig. 6 A) and acidification (Fig. 6 B) were inhibited partially by NPPB (similar results were obtained using 300 μM NPPB). NPPB did not induce H^+ leak under the conditions of these experiments (not depicted). These results support the conclusion that endosomal Cl^- conductance plays an important role in endosomal acidification; however, the data do not provide quantitative information about the role of endosomal Cl^- versus other conductances because of the uncertain percent inhibition of endosomal Cl^- channels by NPPB. Fig. 6 B shows that Cl^- substitution by gluconate produced a more substantial inhibition of endosomal acidification, providing additional evidence for a role of Cl^-. In this experiment, cytosolic [Cl^-] was depleted to <5 mM as shown by SPQ fluorescence measurements. However, it is not possible to deduce quantitative information because of the nonzero permeability of gluconate in the small endosomes (high surface/volume ratio) as well as other phenomena such as endosomal fusion events.

Endosomal H^+ pump activity and K^+ conductance were manipulated to provide more direct information about the contribution of endosomal Cl^- channels to total endosomal ion conductance. Fig. 6 C shows that elevation of endosomal K^+ conductance by valinomycin produced a small increase in the rate of endosomal Cl^- accumulation, probably because of the greater cytoplasmic versus endosomal [K^+]. Fig. 6 C also shows that bafilomycin inhibited Cl^- accumulation in endosomes, suggesting that under normal conditions Cl^- entry into endosomes results from H^+ pumping. Although endosomes must contain significant H^+ conductance, as shown by the reversal of acidification and Cl^- accumulation after late addition of bafilomycin (Fig. 4, A and B, right), the electrochemical driving forces under the conditions in Fig. 6 C prevent significant Cl^- accumulation when H^+ pumping is blocked. However, increasing endosomal K^+ conductance by valinomycin (in the presence of bafilomycin) permitted Cl^- entry (Fig. 6 C), providing direct evidence in J774 cells that endosomal K^+ conductance is very low compared with endosomal Cl^- conductance. As measured by SPQ fluorescence, cytosolic [Cl^-] increased minimally (from 45 to 49 mM) during the 45-min valinomycin incubation.

As a further test of the conclusion that endosomal Cl^- conductance is substantially greater than K^+ conductance under the conditions of our experiments, molar H^+ entry

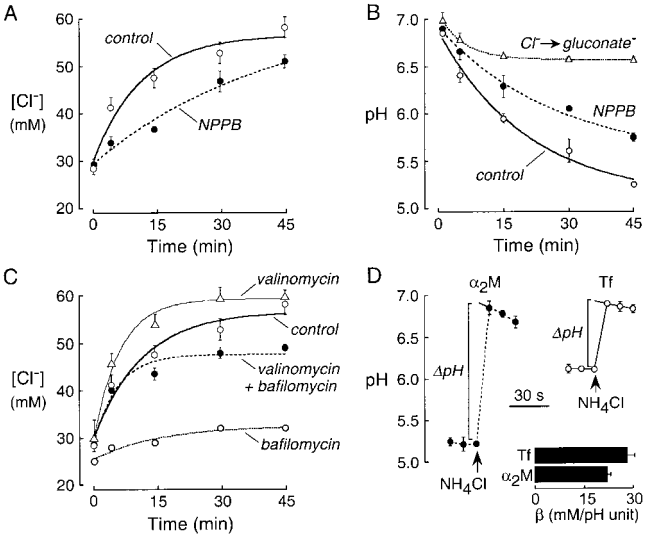

Figure 6. **Role of Cl^- conductance in endosomal acidification.** (A) Inhibition of endosomal Cl^- conductance by NPPB. Kinetics of endosomal $[Cl^-]$ was determined as in Fig. 4 A (right) in PBS (control) and 100 μM PBS-containing NPPB ($n = 4$ sets of experiments). (B) Kinetics of endosomal acidification as in Fig. 4 B (right; $n = 4$). Where indicated, 100 μM NPPB was present in the incubation solution and perfusate. Where indicated, Cl^- was replaced by gluconate for 2 h before experiments and during measurements. (C) Time course of endosomal $[Cl^-]$ was determined as in Fig. 4 A (right), where 10 μM valinomycin and/or 200 nM bafilomycin were present in the incubation solution and perfusate. (D) Representative measurements of endosomal buffer capacity showing the prompt increase in endosomal pH after addition of NH_4Cl to the perfusate.

was related quantitatively to Cl^- entry using endosomal buffer capacity (β) to convert pH change (ΔpH) to molar H^+ entry. Using the NH_4Cl pulse method, the average β was 28 mM/pH unit for Tf-labeled endosomes in the pH range 6.05–6.95 and 22 mM/pH unit for α_2M-labeled endosomes in the pH range of 5.20–6.85 (Fig. 6 D). Thus, the molar quantity of H^+ accumulation in endosomes during a drop in pH from 6.95 to 6.04 for Tf ($\beta \cdot \Delta pH = 25$ mM) agreed well with the molar quantity of Cl^- accumulation (22 mM; Fig. 3 A). For α_2M, the molar quantity of H^+ accumulation ($\beta \cdot \Delta pH = 36$ mM) also agreed with the molar quantity of Cl^- accumulation (31 mM; Fig. 4 A, right). If significant endosomal K^+ exit occurred during acidification, the molar ratio of Cl^-/H^+ transport across the endosomal membrane should be much less than one.

Rapid reduction in endosomal $[Cl^-]$ after endosome formation

As mentioned in the Introduction, an unanticipated finding in our previous measurements of endosomal $[Cl^-]$ using a fluid-phase indicator was the low endosomal $[Cl^-]$ of ~25 mM at the first time point that could be measured, much lower than the $[Cl^-]$ of 137 mM in the extracellular solution. Using fluorescently labeled transferrin, we investigated this phenomenon by first defining the early kinetics of $[Cl^-]$ sensed by BAC-dextran-Tf-TMR after membrane surface labeling and rapidly induced receptor internalization. Fig. 7 A shows BAC and TMR fluorescence micrographs of J774 cells taken at 0–5, 20, and 60 s after internalization at 37°C in presence of PBS (left three panels). Surface labeling was seen at 0–5 s with dim BAC fluorescence because of exposure of BAC-dextran-Tf-TMR to the external solution. Few well-demarcated endosomes were observed by 20 s, though many hazy nascent endosomes were seen having dim BAC fluorescence. Many well-demarcated endosomes were seen by 45–60 s with brighter BAC fluorescence indicating low $[Cl^-]$. In contrast, endosome BAC fluorescence was low (indicating high $[Cl^-]$) at 60 s when internalization was done in low pH buffer (see below) (Fig. 7 A, right panels). Fig. 7 B shows the kinetics of average endosomal $[Cl^-]$ determined by ratio image analysis of individual endosome structures at

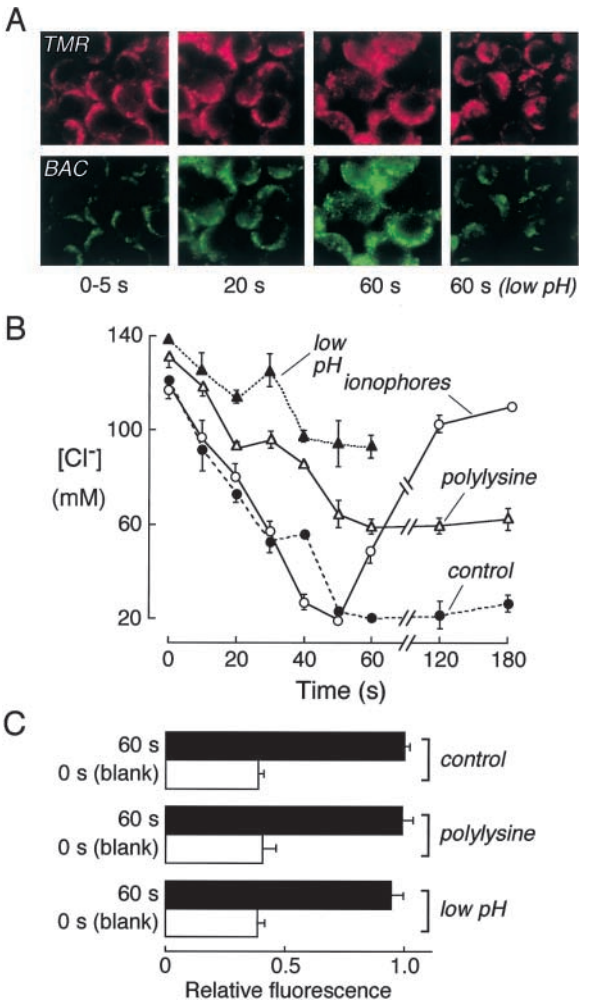

Figure 7. **Early kinetics of endosomal $[Cl^-]$: investigation of the role of Donnan potential.** (A) Fluorescence micrographs (BAC and TMR fluorescence) of cells at indicated times after heating to 37°C. Where indicated (low pH), the 37°C perfusate was at pH 4.0 during internalization. (B) Time course of endosomal $[Cl^-]$ measured using BAC-dextran-Tf-TMR. Where indicated, cells were incubated with polylysine (0.1%, 10,000 kD) at 4°C for 5 min before internalization (polylysine), or a pH 4.0 perfusate was used as in A (low pH), or cells were incubated with high K^+ buffer containing ionophores for 20 min before internalization ($n = 4$). $[Cl^-]$ was measured in individual endosomes/endosome-like structures by ratio image analysis. (C) Rate of endosomal internalization of BAC-dextran-TF-TMR measured from total fluorescence of cell homogenates ($n = 4$). Internalization was done for 1 min as in A, and cells were washed five times at 4°C before homogenization. Blank indicates zero internalization time (heating to 37°C omitted).

indicated times after solution heating to 37°C. [Cl^-] was ~120 mM early after internalization, where ratio imaging was done in blurred endosome-like structures that may or may not represent sealed vesicles. [Cl^-] decreased rapidly to ~20 mM over 60 s. One possible mechanism for the rapid drop in [Cl^-] is a strong interior-negative Donnan potential created by proteins at the inner surface of the endosome-limiting membrane. Other mechanisms include rapid fusion with endosomes containing low [Cl^-] and rapid volume expansion without entry of Cl^- from the cytoplasm. If a negative Donnan potential is responsible, then we reasoned that collapse of the Donnan potential should reduce or prevent the initial drop in [Cl^-]. Two approaches were used to diminish the Donnan potential: inclusion of polylysine after surface labeling to neutralize cell-surface negative charges, and internalization during exposure to a low pH external buffer to protonate anionic proteins at the cell surface.

Fig. 7 B shows that the average [Cl^-] sensed by the BAC-dextran-Tf-TMR decreased to 60 mM in polylysine-treated cells, which was significantly greater than that of 20 mM under control conditions. Under these conditions, average pH sensed by FITC-Tf-TMR at 15–30 s was 6.8–6.9 in control cells and 6.9–7.1 in polylysine-treated cells. Internalization in acidic (pH 4) buffer produced a more marked attenuation of the drop in endosomal [Cl^-] (to 92 mM) than did polylysine treatment, probably because of the greater neutralization of the interior-negative Donnan potential. The early time course of endosomal [Cl^-] in the presence of ionophores/high K^+ showed an initial drop in endosomal [Cl^-] to ~20 mM followed by an increase to cytosolic (external solution) [Cl^-]. The model supported by these findings is that a substantial Donnan potential exists during and just after endosome formation, where endosome volume is small and the concentration of impermeant negative charges is large. In control studies, to determine whether exposure to external polylysine or low pH affected the kinetics of BAC-dextran-Tf-TMR internalization, total cell-associated fluorescence was measured in washed cell homogenates. Fig. 7 C shows that the rate of endosomal internalization over 60 s was not significantly reduced by the low pH or polylysine treatments.

Discussion

This work investigated the kinetics and determinants of [Cl^-] in early/recycling and late endosomes, and in Golgi compartment. The fluorescence labeling strategy involved linking a green-fluorescing Cl^--sensitive dextran containing the BAC chromophore with a red-fluorescing Cl^--insensitive ligand (Tf, α_2M, or CTb) containing the TMR chromophore. The chemistry and purification procedures were established to yield brightly labeled fluorescent ligands with 1:1 dextran/ligand molar stoichiometry. The fluorescent ligands bound to cell-surface receptors with high affinity and were internalized rapidly by receptor-mediated endocytosis. Gel filtration studies of cell homogenates showed that the fluorescent ligands were stable in cells. Fluorescence ratios versus [Cl^-] were calibrated in living cells to permit quantitative determination of [Cl^-] in endosomes and Golgi compartment by ratio imaging fluorescence microscopy. The fluorescent Cl^--sensing ligands represent a substantial technical advance over the fluorescent Cl^--sensing dextran developed previously. The fluorescent ligands are remarkably brighter in cell studies and can be targeted to defined endosomal and Golgi compartments by receptor-mediated internalization using nanomolar dye concentrations.

Fluorescent pH-sensing Tf and α_2M ligands have been used to define the acidification kinetics of endosomes targeted to early/recycling and late endosomal compartments. Tf ligands are targeted to early and recycling endosomes that are relatively alkaline (pH 6.0–6.8) compared with late endosomes and lysosomes (Yamashiro et al., 1984; Yamashiro and Maxfield, 1987; Mellman, 1996). In general, early endosomes accumulate at the cell periphery a few minutes after internalization and later fuse to form recycling endosomes that are distributed near the nucleus. In contrast, α_2M ligands do not recycle to the cell surface but progress rapidly through the endosomal pathway to late, relatively acidic endosomes (pH ~5; Yamashiro et al., 1989; Zen et al., 1992). We found here that the kinetics of Cl^- accumulation in early/recycling and late endosomes approximately paralleled endosomal acidification.

Several lines of functional evidence supported the conclusion that endosomal Cl^- conductance provides the major route for counter ion movement to permit endosomal acidification by electrogenic H^+ pumping. Endosomal Cl^- accumulation was blocked >80% by the vacuolar H^+ pump inhibitor bafilomycin but was restored by the K^+ ionophore valinomycin, providing evidence that intrinsic endosomal K^+ conductance is very low. The molar coupling ratio of H^+ to Cl^- entry was approximately unity, indicating that Cl^- entry rather than K^+ exit accounted for the majority of counter ion movement. Endosomal acidification was remarkably impaired by replacement of Cl^- by gluconate, and endosomal acidification and Cl^- accumulation were inhibited in parallel by a Cl^- channel blocker. In these studies, we made no attempt to define the molecular identity of endosomal Cl^- channel(s), and thus cannot extrapolate our results obtained (mostly J774 and CHO cells) to other cell types where the expression pattern of endosomal ion channels may differ. However, the methods developed here can be readily applied to other systems, such as testing the roles of Cl^- channels ClC-5 in kidney proximal tubule cells or ClC-3 in hippocampal neurons.

[Cl^-] in Golgi compartment was measured by internalization of the ratioable fluorescent conjugate BAC-dextran-CTb-TMR and retrograde transport via the secretory pathway. As found previously for the pH-sensitive fluorescent indicator CF-CTb (Schapiro et al., 1998), the Cl^--sensitive conjugate localized to the Golgi compartment of Vero cells after a 30-min chase time at 37°C. Golgi compartment [Cl^-] was 49 mM and pH was 6.42. This pH is in the range of 5.9–6.7 reported in Golgi compartment of different cell types using a variety of labeling methods (Seksek et al., 1995; Kim et al., 1996; Farinas and Verkman, 1999; Wu et al., 2000; Chandy et al., 2001; Demaurex et al., 1998). Golgi compartment [Cl^-] was insensitive to the cAMP agonist forskolin but decreased substantially after H^+ pump inhibition by bafilomycin and resultant Golgi compartment alkalinization. Inhibition of Golgi compartment H^+ leak by $ZnCl_2$ decreased

the rates of Cl^- exit and alkalinization following bafilomycin. The molar coupling ratio of H^+ to Cl^- exit following bafilomycin was approximately unity, suggesting that Cl^- is the principal counter ion involved in Golgi compartment acidification in Vero cells. This conclusion is somewhat different from that of Demaurex et al. (1998) in a different cell type (CHO cells), where both Cl^- and K^+ contributed to overall Golgi compartment counter ion permeability. Whether cell type or methodological differences account for the different interpretations is unclear. Last, we note that the data here do not address whether Cl^- is an important regulator of steady-state Golgi compartment pH. Indeed, there is good evidence that H^+ leak is high in Golgi compartment and probably a more important determinant of steady-state Golgi pH than Golgi membrane potential (Kim et al., 1996; Farinas and Verkman, 1999; Wu et al., 2000).

The low endosomal [Cl^-] just after internalization was an intriguing observation because the aqueous lumen of a nascent endosome is exposed to a high extracellular [Cl^-] at the time of internalization. The kinetic data here show that the [Cl^-] sensed by the fluorescently labeled transferrin ligand was initially >120 mM before internalization but decreased rapidly to ~20 mM ($t_{1/2} \approx 30$ s) after initiation of internalization. The reduction in [Cl^-] was not inhibited by NPPB, suggesting that Cl^- transport across the endosomal membrane is not involved in this process. We tested the hypothesis that the low [Cl^-] is related to the interior-negative Donnan potential produced by negative charges on membrane proteins that face the outside solution when at the plasma membrane and the lumen after endosome formation. Partial neutralization of surface charge by inclusion of polylysine after ligand binding resulted in increased endosomal [Cl^-]. Conversion of the surface charges from negative to positive by exposure to pH 4.0 buffer at the time of endosome formation prevented the low [Cl^-] observed under control conditions, without changing the rate of dye internalization. These results support the hypothesis that the initial low [Cl^-] is produced by an interior-negative Donnan potential.

The low [Cl^-] and aqueous volume in endosomes early after internalization provides a simple and elegant mechanism to permit endosomal acidification without lysis. We propose that endosomes form as flattened structures with very high surface/volume ratio and hence a substantial interior-negative Donnan potential. [Cl^-] in nascent endosomes is low compared with that in the external solution just as endosomes form. Active H^+ entry by the vacuolar proton pump is accompanied by secondary active Cl^- entry to maintain electroneutrality. The chemical gradient of Cl^- from cytoplasm (generally 30–70 mM) to early endosomes (~20 mM) provides a favorable electrochemical driving force for Cl^- entry in response to H^+ pumping. The Donnan potential decreases as endosomes acidify (titrating fixed negative charges) and accumulate ions by transport and fusion events. To achieve full acidification in late endosomes, the H^+ entry is accompanied by a substantial increase in [Cl^-]. The low [Cl^-] after internalization, thus, permits the acidification-driven increment in [Cl^-] without development of a large opposing (endosome to cytoplasm) Cl^- gradient. Furthermore, the low internal aqueous volume of the nascent endosome permits the accumulation of osmoles and, thus, water without reaching a critical volume where endosome lysis occurs. Validation of our hypothesis will require measurements of endosomal membrane potential, volume, and K^+ concentration in order to define the electrochemical forces driving protons, ions, and water across the endosomal membrane.

Materials and methods

Chemicals

Unless otherwise indicated, chemicals were purchased from Sigma-Aldrich. FITC, TMR–succinimidyl ester, and amino dextran (40 kD) were obtained from Molecular Probes Inc. BAC–succinimidyl ester was synthesized as described previously (Sonawane et al., 2002).

Cell culture

J774.1 macrophages (ATCC No. TIB-67) were obtained from American Type Culture Collection and grown in DME-H21. CHO-K1 cells (ATCC No. CCL-61) were grown in Ham's F-12K medium, and Vero cells (ATCC No. CCL-81) were grown in MEM containing 2 mM glutamine. All media were supplemented with 10% fetal bovine serum, 100 U/ml penicillin, and 100 μg/ml streptomycin. Cells were cultured on 18-mm-diam round coverslips at 37°C in 95% air/5% CO_2, and used just before confluence.

Synthesis of fluorescently labeled ligands for [Cl^-] measurements

Synthesis of TMR-Tf-SH and TMR-α_2M-SH (Fig. 1 A, left). A mixture of diferric Tf (14 nM in 1 ml PBS) or α_2M (7.1 nM in 2 ml PBS) and TMR-succinimidyl ester (40 nM, from DMSO stock solution) were stirred slowly at room temperature for 1 h. Unreacted dye was removed by gel filtration (Sephadex G25, PBS). Using molar absorbance data, dye/protein ratios were 2.1:1 (TMR-Tf) and 2.4:1 (TMR-α_2M). Equal volumes of diferric TMR-Tf or TMR-α_2M (10 μM in degassed PBS) and iminothiolane (13 μM PBS containing 5 mM EDTA, pH 8) were mixed and incubated for 1 h at room temperature in the dark under N_2. Unreacted iminothiolane was removed by gel filtration (Sephadex G25). Sulfhydryl group/ligand molar labeling ratios were 0.91:1 (TMR-Tf-SH) and 0.96:1 (TMR-α_2M-SH) as measured using Ellman's reagent (extinction coefficient 13,600 $M^{-1}cm^{-1}$, 412 nm). No ligand polymerization was found by SDS-PAGE.

Synthesis of BAC-dextran-S-S-2Py. 5 μM amino dextran (40 kD) was stirred with 7 μM SPDP in 20 ml aqueous $NaHCO_3$ (0.1 M, pH 8) at room temperature for 1 h. The dextran conjugate was dialyzed (25-kD cut-off) for 24 h against 0.1 M $NaHCO_3$, and then against 10 mM PBS for 36 h at 4°C. The pyridyl/dextran molar labeling ratio was 0.95 as measured by liberation of pyridine-2-thion after reduction (extinction coefficient, 8,100 $M^{-1}cm^{-1}$; 343 nm). 5 μM purified amino dextran-S-S-2Py was reacted with 50 mM BAC–succinimidyl ester (prepared as per Sonawane et al., 2002) in 50 ml aqueous $NaHCO_3$ (0.1 M, pH 8) at room temperature for 3 h. The reaction mixture was dialyzed and concentrated for conjugation with TMR-Tf-SH or TMR-α_2M-SH.

Synthesis of BAC-dextran-Tf-TMR and BAC-dextran-α_2M-TMR. 7 nM TMR-Tf-SH or 7 nM TMR-α_2M-SH was mixed with BAC-dextran-S-S-2Py (8.8 nM in 2 ml PBS containing 5 mM EDTA, pH 8) and incubated for 18 h at room temperature under N_2. Unreacted TMR-Tf-SH (or TMR-α_2M-SH) and BAC-dextran-S-S-2Py were removed by gel filtration (Sephadex G-100). BAC-dextran-Tf-TMR and BAC-dextran-α_2M-TMR were lyophilized and stored at −20°C in a dessicator in the dark.

Synthesis of BAC-dextran-CTb-TMR (Fig. 1 A, right). TMR-CTb was synthesized as described above for TMR-Tf (TMR/CTb molar ratio, 2.2:1). Equal volumes of TMR-CTb (10 μM, PBS) and MBS (13 μM in PBS, pH 7) were incubated for 1 h at room temperature in the dark under N_2. Unreacted MBS was removed by gel filtration (Sephadex G25). The maleimide benzoyl group/ligand molar labeling ratio was 0.96:1. BAC-dextran-S-S-2Py (synthesized above) was reduced with mercaptoethanol (1:3 molar excess) for 1 h to give BAC-dextran-SH which was purified by dialysis (25-kD cut-off) against 10 mM PBS containing 5 mM EDTA for 20 h at 4°C. TMR-CTb-MB (77 nM, 0.5 ml PBS) was mixed with BAC-dextran-SH (88 nM in 2 ml PBS containing 5 mM EDTA, pH 7) and incubated for 10 h at room temperature under N_2. Unreacted TMR-CTb-SH and BAC-dextran-SH were removed by gel filtration (Sephadex G-100). BAC-dextran-CTb-TMR was lyophilized and stored at −20°C.

Synthesis of fluorescently labeled ligands for pH measurements

TMR-Tf or TMR-α_2M (5 nM) as prepared above were mixed with FITC (50 nM from DMSO stock) in 1 ml aqueous $NaHCO_3$, pH 8, and gently

stirred for 1 h. The reaction products FITC-Tf-TMR and FITC-α_2M-TMR were purified by gel filtration chromatography (Sephadex G-25). Thin layer chromatography showed no free dye contamination of the fluorescently labeled ligands. Molar labeling ratios were 5.1:1:2.1 (FITC/Tf/TMR) and 5.8:1:2.4 (FITC/α_2M/TMR). CF-CTb-TMR was synthesized and purified identically, except that carboxyfluorescein (CF) succinimidyl ester was used in place of fluorescein isothiocynate. Molar labeling ratio was 4.9:1:2.2 (CF/CTb/TMR).

Characterization of the ratioable fluorescent Cl^- ligands

Molecular masses of the conjugates (before and after cell internalization) were determined by column chromatography (Sephacryl 300HR). Eluted fractions were assayed for BAC and TMR fluorescence. Fluorescence spectra, molar extinction coefficients, and quantum yields were measured using a fluorimeter (Fluoromax-3). In fluorescence quenching studies, microliter aliquots of NaCl (1-M stock) were added to 3 ml of fluorescent ligand (10 μM in 5 mM Na_2HPO_4-NaH_2PO_4, pH 7.4). Stern-Volmer constant (K_{sv}) was calculated from the slope of $F_0/F - 1$ versus [Cl^-] plots ($F_0/F - 1 = K_{sv}$ [Cl^-]), where F_0 is BAC fluorescence in the absence and F in the presence of Cl^-.

Endosome labeling and kinetics of endosomal [Cl^-] and pH

Cells were incubated in serum-free medium for 15 min at 37°C before experiments. For receptor-mediated endocytosis, the cell surface was labeled by incubation with the Cl^- or pH indicators (300 nM for Tf, 100 nM for α_2M) for 15 min in PBS (containing 1 mM $CaCl_2$ and $MgCl_2$) at 4°C. Coverslips were washed twice with ice-cold PBS and transferred to a precooled perfusion chamber (0°C) containing ice-cold perfusate. Sets of BAC and TMR images (for Cl^-) or FITC and TMR images (for pH) were acquired at specified times after rapid warming by perfusion at 37°C in a microincubator (PDMI-2; Harvard Apparatus). In some experiments, the perfusate contained 200 nM bafilomycin A_1, 5–30 mM NH_4Cl, 10 μM valinomycin, 100 μM NPPB, or 5 mM acetate or pthalate buffer, pH 4. In Cl^--free experiments, perfusate Cl^- was replaced by gluconate and cells were incubated with the Cl^--free perfusate for 2 h before measurements. In some experiments, cells were incubated in polylysine solution (0.1% in PBS) at 4°C for 5 min before experiments. In some experiments, the 37°C perfusate was titrated to pH 4.0 to alter surface protein charge. In some experiments, cells were pretreated with 200 μM ouabain in PBS for 20 min.

Golgi compartment [Cl^-] and pH

Cells were incubated in serum-free medium for 30 min at 37°C, washed three times with ice-cold PBS, and incubated with Cl^- or pH indicators (200 nM) for 30 min in PBS at 4°C. Coverslips were washed three times with ice-cold PBS, warmed, and maintained at 37°C for 45 min, which is when a typical Golgi compartment pattern was observed. Sets of BAC and TMR images (for Cl^-) or CF and TMR images (for pH) were acquired. In some experiments, the perfusate contained 200 nM bafilomycin, 5–20 mM NH_4Cl, or 200 μM $ZnCl_2$.

Calibration protocols

For in vivo Cl^- calibrations (BAC/TMR fluorescence ratio vs. [Cl^-]), perfusate and endosomal [Cl^-] were equalized by incubating cells for 15–20 min at 37°C in 120 mM KCl/KNO_3, 20 mM NaCl/$NaNO_3$, 1 mM $CaCl_2$, 1 mM $MgCl_2$, 10 mM HEPES, pH 7.4, with [Cl^-] from 0 to 120 mM (NO_3^- replacing Cl^-). Solutions contained the ionophores nigericin (10 μM), valinomycin (10 μM), CCCP (5 μM) and monensin (10 μM), and the H^+ pump inhibitor bafilomycin (200 nM). For in vivo pH calibrations (TMR/FITC fluorescence ratio vs. pH), cells were incubated with high K^+ solutions containing nigericin, valinomycin, and bafilomycin, pH adjusted to 4–8. For calibration of Golgi compartment Cl^- and pH indicators, Vero cells were incubated with calibration buffers at 45 min after internalization.

Endosomal and Golgi compartment buffer capacity

Buffer capacity (β) was determined from the rapid increase in endosomal/Golgi compartment pH in response to addition of 5–30 mM NH_4Cl to the perfusate. β was computed from the equation:

$$\beta = ([NH_4Cl]/\Delta pH) \cdot 10^{(pH_{out} - pH_{final})},$$

where ΔpH is the pH increase just after NH_4Cl addition, pH_{out} is perfusate pH, and pH_{final} is endosomal/Golgi compartment pH after addition of NH_4Cl determined by extrapolation of the pH time course to the time of NH_4Cl addition. [NH_4Cl] was chosen to give the same pH increase as that produced by bafilomycin.

Fluorescence microscopy

Experiments were performed using a Leitz upright fluorescence microscope equipped with a coaxial-confocal attachment and 14-bit cooled (−30°C) charge-coupled device camera as described previously (Zen et al., 1992). Cells were initially identified and focused using dim red light to avoid photobleaching. Fluorescence was collected using a 100× oil immersion objective (numerical aperture, 1.4; Plan-Apo [Nikon]). Images (500-ms acquisition time) were obtained using a custom filter set for BAC (excitation 470 ± 5 nm, dichroic 505 nm, emission 535 ± 20 nm), and standard TMR and FITC filter sets. Serial image acquisitions indicated <3% BAC photobleaching per image acquisition, and <1% photobleaching for TMR and FITC. In time course studies, endosomes in different cells were imaged for different time points except where indicated.

Ratio image analysis

Custom software was written in Labview to compute area-integrated background-subtracted pixel intensities as described previously (Sonawane et al., 2002). Four regions of cells containing well-demarcated endosomes were identified by rectangular boxes in each TMR (red) image; for each region, four nearby regions outside of the endosome/cell were identified for background determination. The same regions were identified automatically in the BAC or FITC (green) image. After background subtraction, R/G intensity ratios were computed from area-integrated intensities. Three pairs of images were analyzed for each time point. Similarly, background-subtracted intensities of BAC (or CF) and TMR were determined for a labeled perinuclear region of well-defined Golgi compartments for computation of R/G. For studies of the early kinetics of endosomal [Cl^-], R/G was determined in individual endosomes. Area-integrated intensities of individual endosomes were calculated using a rectangular annular region just outside of the endosome-containing rectangle as a background (Zen et al., 1992).

This work was supported by grants EB00415, HL59198, DK35124, HL60288, and EY13574 from the National Institutes of Health, and grant R613 from the Cystic Fibrosis Foundation.

Submitted: 21 November 2002
Revised: 11 February 2003
Accepted: 12 February 2003

References

Bae, H.R., and A.S. Verkman. 1990. Protein kinase A regulates chloride conductance in endocytic vesicles from proximal tubule. *Nature.* 348:637–639.

Busch, G.L., H.J. Lang, and F. Lang. 1996. Studies on the mechanism of swelling-induced lysosomal alkalinization in vascular smooth muscle cells. *Pflügers Arch.* 431:690–696.

Cain, C.C., D.M. Sipe, and R.F. Murphy. 1989. Regulation of endocytic pH by the Na^+,K^+-ATPase in living cells. *Proc. Natl. Acad. Sci. USA.* 86:544–548.

Chandy, G., M. Grabe, H.P. Moore, and T.E. Machen. 2001. Proton leak and CFTR in regulation of Golgi pH in respiratory epithelial cells. *Am. J. Physiol. Cell Physiol.* 281:C908–C921.

Dautry-Varsat, A. 1986. Receptor-mediated endocytosis: the intracellular journey of transferrin and its receptor. *Biochimie.* 68:375–381.

Demaurex, N., W. Furuya, S. D'Souza, J.S. Bonifacino, and S. Grinstein. 1998. Mechanism of acidification of the trans-Golgi network (TGN). In situ measurements of pH using retrieval of TGN38 and furin from the cell surface. *J. Biol. Chem.* 273:2044–2051.

Farinas, J., and A.S. Verkman. 1999. Receptor mediated targeting of fluorescent probes in living cells. *J. Biol. Chem.* 274:7603–7606.

Fuchs, R., P. Male, and I. Mellman. 1989a. Acidification and ion permeabilities of highly purified rat liver endosomes. *J. Biol. Chem.* 264:2212–2220.

Fuchs, R., S. Schmid, and I. Mellman. 1989b. A possible role for Na^+,K^+-ATPase in regulating ATP-dependent endosome acidification. *Proc. Natl. Acad. Sci. USA.* 86:539–543.

George, A.L. 1998. Chloride channels and endocytosis: ClC-5 makes a dent. *Proc. Natl. Acad. Sci. USA.* 95:7843–7845.

Glickman, J., K. Croen, S. Kelly, and Q. Al-Awqati. 1983. Golgi membranes contain an electrogenic H^+ pump in parallel to a chloride conductance. *J. Cell Biol.* 97:1303–1308.

Grabe, M., and G. Oster. 2001. Regulation of organelle acidity. *J. Gen. Physiol.* 117:329–344.

Hogemann, D., L. Josephson, R. Weissleder, and J.P. Basilion. 2000. Improvement of MRI probes to allow efficient detection of gene expression. *Biocon-*

jug. Chem. 11:941–946.

Jentsch, T.J., V. Stein, F. Weinreich, and A.A. Zdebik. 2002. Molecular structure and physiological function of chloride channels. *Physiol. Rev.* 82:503–568.

Kim, J.H., C.A. Lingwood, D.B. Williams, W. Furuya, M.F. Manolson, and S. Grinstein. 1996. Dynamic measurement of the pH of the Golgi complex in living cells using retrograde transport of the verotoxin receptor. *J. Cell Biol.* 134:1387–1399.

Kornak, U., D. Kasper, M.R. Bosl, E. Kaiser, M. Schweizer, A. Schulz, W. Friedrich, G. Delling, and T.J. Jentsch. 2001. Loss of the ClC-7 chloride channel leads to osteopetrosis in mice and man. *Cell.* 104:205–215.

Marshansky, V., and P. Vinay. 1996. Proton gradient formation in early endosomes from proximal tubules. *Biochim. Biophys. Acta.* 1284:171–180.

Mellman, I. 1996. Endocytosis and molecular sorting. *Annu. Rev. Cell Dev. Biol.* 12:575–625.

Mukherjee, S., R.N. Ghosh, and F.R. Maxfield. 1997. Endocytosis. *Physiol. Rev.* 77:759–803.

Mulberg, A.E., B.M. Tulk, and M. Forgac. 1991. Modulation of coated vesicle chloride channel activity and acidification by reversible protein kinase A-dependent phosphorylation. *J. Biol. Chem.* 266:20590–20593.

Piwon, N., W. Gunther, M. Schwake, M.R. Bosl, and T.J. Jentsch. 2000. ClC-5 Cl^--channel disruption impairs endocytosis in a mouse model for Dent's disease. *Nature.* 408:369–373.

Rybak, S.L., F. Lanni, and R.F. Murphy. 1997. Theoretical considerations on the role of membrane potential in the regulation of endosomal pH. *Biophys. J.* 73:674–687.

Schapiro, F.B., and S. Grinstein. 2000. Determinants of the pH of the Golgi complex. *J. Biol. Chem.* 275:21025–21032.

Schapiro, F.B., C. Lingwood, W. Furuya, and S. Grinstein. 1998. pH-independent retrograde targeting of glycolipids to the Golgi complex. *Am. J. Physiol.* 274: C319–C332.

Schmid, A., G. Burckhardt, and H. Gogelein. 1989. Single chloride channels in endosomal vesicle preparations from rat kidney cortex. *J. Membr. Biol.* 111: 265–275.

Seksek, O., J. Biwersi, and A.S. Verkman. 1995. Direct measurement of trans-Golgi pH in living cells and regulation by second messengers. *J. Biol. Chem.* 270:4967–4970.

Sonawane, N.D., J.R. Thiagarajah, and A.S. Verkman. 2002. Chloride concentration in endosomes measured using a ratioable fluorescent Cl^- indicator: evidence for chloride accumulation during acidification. *J. Biol. Chem.* 277: 5506–5513.

Stobrawa, S.M., T. Breiderhoff, S. Takamori, D. Engel, M. Schweizer, A.A. Zdebik, M.R. Bosl, K. Ruether, H. Jahn, A. Draguhn, et al. 2001. Disruption of ClC-3, a chloride channel expressed on synaptic vesicles, leads to a loss of the hippocampus. *Neuron.* 29:185–196.

Van Weert, A.W., K.W. Dunn, H.J. Gueze, F.R. Maxfield, and W. Stoorvogel. 1995. Transport from late endosomes to lysosomes, but not sorting of integral membrane proteins in endosomes, depends on the vacuolar proton pump. *J. Cell Biol.* 130:821–834.

Wagner, E., M. Zenke, M. Cotten, H. Beug, and M.L. Birnstiel. 1990. Transferrin-polycation conjugates as carriers for DNA uptake into cells. *Proc. Natl. Acad. Sci. USA.* 87:3410–3414.

Wu, M.M., J. Llopis, S. Adams, J.M. McCaffery, M.S. Kulomaa, T.E. Machen, H.P. Moore, and R.Y. Tsien. 2000. Organelle pH studies using targeted avidin and fluorescein-biotin. *Chem. Biol.* 7:197–209.

Wu, M.M., M. Grabe, S. Adams, R.Y. Tsien, H.P. Moore, and T.E. Machen. 2001. Mechanisms of pH regulation in the regulated secretory pathway. *J. Biol. Chem.* 276:33027–33035.

Yamashiro, D.J., and F.R. Maxfield. 1987. Kinetics of endosome acidification in mutant and wild-type Chinese hamster ovary cells. *J. Cell Biol.* 105:2713–2721.

Yamashiro, D.J., B. Tycko, S.R. Fluss, and F.R. Maxfield. 1984. Segregation of transferrin to a mildly acidic (pH 6.5) para-Golgi compartment in the recycling pathway. *Cell.* 37:789–800.

Yamashiro, D.J., L.A. Borden, and F.R. Maxfield. 1989. Kinetics of alpha 2-macroglobulin endocytosis and degradation in mutant and wild-type Chinese hamster ovary cells. *J. Cell. Physiol.* 139:377–382.

Zen, K., J. Biwersi, N. Periasamy, and A.S. Verkman. 1992. Second messengers regulate endosomal acidification in Swiss 3T3 fibroblasts. *J. Cell Biol.* 119: 99–110.